Rev. LatinAm. Metal. Mat.

Artículo Regular

www.rlmm.org

CORROSION RESISTANCE OF FERROUS COATINGS PRODUCED BY THERMAL SPRAY

Edwin López, Jairo Olaya1*

Departamento de Ingeniería Mecánica y Mecatróncia, Universidad Nacional de Colombia, Bogotá, Colombia.

**e-mail: ealopezco@unal.edu.co*, jjolayaf@unal.edu.co*

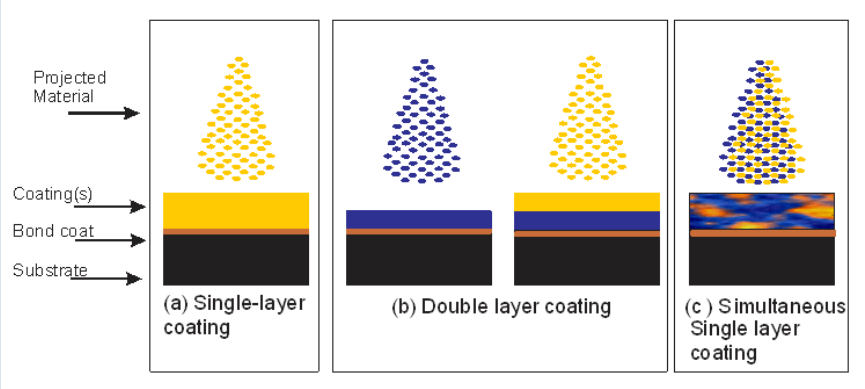

ABSTRACT

Three materials were deposited on AISI-SAE 4340 steel using the wire arc thermal spray technique. The deposited materials are commercially known as 140MXC (Fe, Nb, Cr, W), 530AS, which is a steel similar to AISI-SAE 1015, and 560AS, which is a steel similar to AISI-SAE 420. With the aim of evaluating the best strategy for increasing the corrosion resistance in the coating-substrate system, the coatings were deposited in three different ways: (1) homogeneous monolayers (single layers) of each material, (2) (Double layer) bilayers composed of a monolayer of 140MXC over a monolayer of either 530AS or 560AS, and (3) simultaneous monolayer-type (single layer) coatings achieved by depositing 140MXC + 530AS in the first case and 140MXC + 560AS in the second case. The coatings were characterized by optical microscopy and X-ray diffraction. The corrosion resistance was evaluated using electrochemical impedance spectroscopy and potentiodynamic polarization. The resistance to polarization of the material deposited in bilayers was increased through the congestion of defects with corrosion products, while the simultaneous monolayers achieved increased corrosion resistance by the reduction of defects with respect to 140MXC. The details and mechanisms of corrosion in the fabricated coatings are described in this study.

Keywords: Thermal spray, Corrosion, Nanocomposites, Multilayers, Pseudo-alloying.

RESISTENCIA A LA CORROSIÓN DE RECUBRIMIENTOS FERROSOS PRODUCIDOS POR PROYECCIÓN TÉRMICA

RESUMEN

Mediante proyección térmica de arco eléctrico fueron depositados tres materiales comercialmente conocidos como: 140MXC (a base de Fe, W, Cr, Nb), 530AS (acero AISI 1015) y 560AS (acero AISI 420), sobre acero AISI 4340. Con el objetivo de evaluar la mejor estrategia para incrementar la resistencia a la corrosión en el sistema capa-sustrato, los recubrimientos fueron depositados de tres formas: (1) Monocapas homogéneas de cada material; (2) bicapas compuestas de una monocapa de 530AS o de 560AS y la segunda de1 140MXC en ambos casos y (3) recubrimientos tipo monocapa el primero depositando de manera simultánea 140MXC + 530AS y otro depositando de manera simultánea 140MXC + 560AS. La microestructura de los recubrimientos fue caracterizada mediante difracción de rayos X. Fue evaluada la resistencia a la corrosión mediante espectroscopía de impedancia electroquímica y polarización potenciodinámica.

La resistencia a la polarización de los recubrimientos bicapas aumentó mediante el depósito de los productos de corrosión en los defectos del recubrimiento, mientras que en las monocapas disimiles aumentó la resistencia a la corrosión por la reducción de defectos, con respecto al recubrimiento 140MXC. Los detalles y mecanismos de corrosión de los recubrimientos producidos se describen en esta investigación.

Palabras clave: Proyección térmica, Corrosión, Nanocompositos, Multicapas, Seudo-aleaciones.

1. INTRODUCTION

Thermal spray processing consists of the deposition of molten and semi-molten particles on a substrate within a short period of time to minimize the contact of the particles with oxidizing agents, such as environmental air [1-2]. When these particles are deposited on the substrate, they become deformed, generating a compact microstructure formed by lenticular sheets called "splats." These splats stack upon each other and coalesce rapidly, thereby forming the thermal spray coating [3]. This type of coating is typically characterized as polycrystalline and uniform, and it can be applied to improve the properties of surfaces or to restore parts that have become worn during service. This deposition method involve material transport techniques, such as flame, electric arc, high velocity oxy-fuel, and plasma [4]. New materials have also been developed to possess different chemical compositions and arrangements, such as wires, powders or powder-filled wires. The combination of these techniques and materials produces a great variety of industrial and research applications.

The electric arc thermal spray technique consists of transporting two electrically charged wires with opposite polarities into a gun and then bringing the wires closer together at a constant speed, forming an electric arc that melts the wires. At the same time, a stream of compressed air is passed at high speed through the arc; this process atomizes and drags the molten material toward the surface of the substrate. A significant variety of coating materials are available on the market for this technique in the form of wires. These products can be differentiated by their depositional properties and chemical compositions, hence it is possible to find a variety of products, which range from simple carbon steels to complex alloys of unknown composition. Each wire is designed to meet the demands of specific applications and must be deposited according to specific parameters, such as the current, the potential, and the compressed air pressure [5-8].

The use of wire arc spraying technology as a coating deposition method has been previously studied [9]. It has been found that this deposition method is useful for the coating of large areas in a short time. Additionally, wire arc spray coatings can be applied to different materials, in different thicknesses and with a significant variety of filler materials. One filler material is a Fe-Cr-W-Nb alloy, which is commercially known as 140MXC and is recommended for the protection of materials from corrosive environments and from the risk of abrasive wear. Its properties are due to the alloying elements and the nanocomposite structure obtained during the coating process. The carbon steel AISI-SAE 1020 is a material of significant technological interest that can be deposited by the thermal spray technique and is commercially available with a similar composition as 530AS. This low-carbon steel is characterized by its low hardness and reduced mechanical resistance and is therefore often used in applications of low mechanical risk or as a mechanical fuse. It is also often used as a filler or disposable coating material. Finally, another material that can be used with the electric arc technique is stainless steel AISI-SAE 420, which is of martensitic nature due to its chromium content and is commercially available as 560AS. This material is characterized as possessing a medium hardness relative to other steels and as forming a passive layer of chromium oxide in the presence of some mediums, which makes it ideal for applications in corrosive environments. It is also possible to find this material in use within some moderate wear applications or as filler.

The development of bilayers and monolayers of dissimilar materials can be achieved with techniques such as physical vapor deposition (PVD) or chemical vapor deposition (CVD). However, these architectures tend to be poorly developed and have been little studied in thermal spray processes. Only a few investigations have used powders [10-11], which simplify the control of the precursor mixture as it is fed into the feeding hopper. Fewer studies have approached these material combinations with the use of electric arc. For example, some coatings have been made with Zn, Al, and AISI-SAE 316L for the formation of bilayers [12]. The fabrication of simultaneous layers of Al, Cu, or Zn has also been explored in the formation of pseudo-alloys (mechanical mixing) and partial alloys [13].

The purpose of this investigation is to use electric arc thermal spray technology to obtain monolayers and bilayers of 140MXC, 530AS and 560AS commercial coatings over AISI 4340 steel. Moreover, the corrosión resistance is investigated using electrochemical impedance spectroscopy tests and potentiodynamic polarization; the resulting microstructures are characterized by X-ray

©2014 Universidad Simón Bolívar

diffraction as well as optical technique.

2. EXPERIMENTAL PART

Coatings were produced by the thermal spray technique using the following materials: (1) 140MXC iron-based tubular wire filled with powders of Cr, W, and Nb; (2) 530AS wire of a composition similar to AISI 1020; and (3) 560AS wire of a composition similar to AISI 420. Prior to the deposition of these materials, an intermediate coating was fabricated with an alloy of nickel 5% aluminum in order to increase the adhesion between subtract and coatings. The deposition strategies were classified as shown in Figure 1, including three separate coatings or independent single layer of 140MXC, 530AS, and 560AS as well as 10 bilayer-type coatings, i.e., 5 with 530AS at the bottom and 140MXC at the top (140MXC/530AS) and 5 with 560AS at the bottom and 140MXC at the top (140MXC/560AS). In both cases, each of the coatings had a different thickness. Finally, two monolayer coatings were produced simultaneously using dissimilar wires of 140 MXC+530AS in the first case and 140MXC+560AS in the second case. The bond coating had an average thickness of 30 µm, plus the coatings, all of them had a total average thickness of 600 µm as shown in Figure 1 specifically the double layer coatings were two different groups of coatings made with two different coatings in the bottom that increase the thickness in average 100 µm in each treatment and top coatings that reduce his thickness in the same way in each treatment. For example the first treatment begin with a layer of 530AS or 560AS of 100 µm and above it one layer of 500 µm of 140MXC, the second treatment was a layer of 200 µm of 530AS or 560AS and above it one layer of 140MXC of 400 µm, so on until the fifth treatment with a first layer of 530AS or 560AS of 500 µm and above it one layer of 140MXC of 100 µm on top. All coatings were deposited on AISI 4340 steel substrates quenched and tempered that were measured to have approximately 5 GPa of hardness [14], the substrate were polished by abrasive discs until reaching an average roughness (Ra) of 0.5 µm, cleaned with isopropanol and acetone in ultrasonic immersion, blasted with aluminum oxide of purity 96.04%, mesh 30 and 413 kPa of pressure [15-17], consuming an average of 3.108 cm^3/cm^2 of aluminum oxide until obtaining a white metal with an average roughness (Ra) of 2.2 µm.

The materials were deposited by electric arc thermal spray using the equipment System 4 Eutectic. Table 1 shows the values of the deposition parameters recommended by the manufacturers [3-5]; these values are common to all materials including the bond coat, also all the wires have a diameter of 1.6 mm and the feed rate was between 5,5 and 6,5 cm/s.

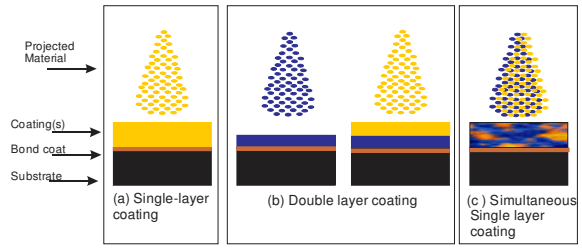

Figure 1. The application methodology for fabricating monolayers, bilayers and simultaneous monolayers.

Table 1. The deposition parameters used for the 140MXC, 530AS, 560AS and 500AS thermal spray coatings.

Deposition Parameters		Values
Air Pressure (MPa)	*Primary*	*413*
	Secondary	*275*
Voltage (V)		*30*
Current (A)		*175*
Spraying distance (cm)		*10.12*

To deposit the coatings, the substrates were placed directly onto a thin metal foil with magnets on the back, which adhered the film-coated substrates to the foil during the coating process. The thickness of each sample was measured before and after each deposition using a caliper gauge, and the increased thickness of the coatings was determined by taking the differences of the measurements.

Corrosion tests were performed using a GAMRY Instruments Reference 600 potentiostat-galvanostat in accordance with ASTM G3 and G5 standards [18-19]. A high purity graphite counter electrode and a reference saturated calomel electrode (SCE) were used. The exposed area was approximately 0.196 cm^2; the electrolyte was a 3% w/v NaCl analytical grade reagent solution made with distilled and deionized water, pH 6.030, at room temperature. The polarization was performed after two hours of immersion, respect to the resting potential between -0.5 V and 0.7 V at a rate of 30 mV/min. The electrochemical impedance spectroscopy test was

performed at 2, 24, 46 and 168 hours following the placement of the sample in the electrolyte. The tests were conducted between 0.01 Hz and 100,000 Hz and an overpotential of 10 mV.

Microstructural characterization was performed by X-ray diffraction using an X'Pert PRO PANalytical diffractometer in Bragg-Brentano geometry with a Kα copper monochromatic line (1.540998 Å) at 45 kV and 40 mA. Optical microscopy observations were performed on a LECO metallographic microscope on samples cut in cross section of the coating using cooled cutting and polishing with aluminum oxide in aqueous suspension until mirror shine.

3. RESULTS AND DISCUSSION

Figure 2 shows the XRD patterns of the types of coatings produced. For coating 140MXC, a single low intensity signal can be observed. This signal may correspond to crystalline iron and/or an amorphous iron formation, which may have formed as a result of the high cooling rates; alternative causes may be the size of the powders, which can act as nano-crystal nucleators, contained in the wire or the pressure and flow characteristics of the air atomizing the molten material to nanometric size. Other studies [22] have identified this type of formation in 140MXC as randomly oriented nanocrystalline grains embedded in an amorphous matrix. This same spectrum appears for the 140 MXC/530AS and 140MXC/560AS bilayers, possibly as a result of the layer thickness, which is greater than 50 µm; this thickness could have caused the incident X-ray beam to penetrate the shell only at the top layer of coating.

In the monolayer coatings of 530AS and the dissimilar 140MXC+530AS, the bcc alpha iron structure was identified based on a mixed orientation of the (200), (211), and (110) planes. It also can be observed that the 140MXC+530AS specimen exhibits a weaker signal intensity close to 45°. This observation can be attributed to the combination of materials and their respective diffraction signals. The spectrum found in the 530AS diffractogram is consistent with the spectrums reported in other studies, which utilized the same low carbon steel deposited by electric arc [8]. The specimen 560AS exhibited bcc deformed in one of its edges forming FeCr HCP structure with the same orientations of 530AS, , which is in good agreement with the results reported in other studies [5]. The intensities of these signals decreased with the addition of 140MXC wire in the coating due also to the combination of materials.

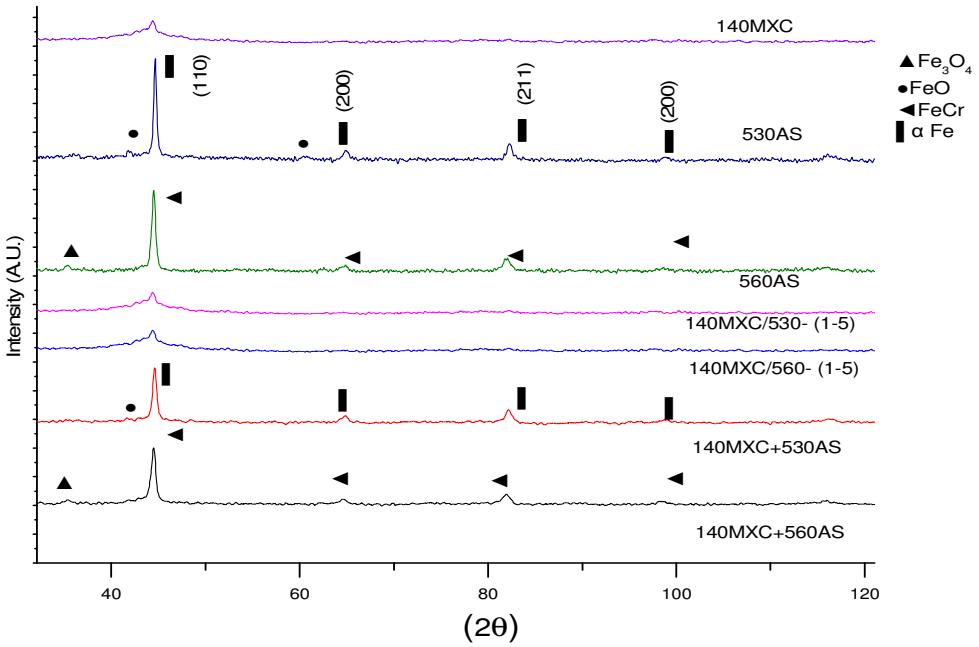

Figure 2. The X-ray diffraction patterns of the coatings produced.

The Figure 3 shows the optical microscopy cross-sections of some of the obtained coatings. The material constituents were differentiated by chemical attack with Nital for 530AS and Vilella's reagent for 560AS [20]. Alloy 140MXC was not attacked with the traditional reagents and appear white.

The top of first column ofFigure 3 shows the monolayer coating of 140MXC in which surface and internal microcracks as well as holes and micropores are visible those defects are also seen in the cross-sections of double layers with the 140MXC in the top. A well-defined interface between coatings and fissure formations appears; additionally, microvoids can be identified in association with the deposition of 140MXC, finally in the simultaneous single layer coatings can be seen the mixture of both deposited materials and a significant decrease in the defects. On the other hand single layers of 530AS and 560AS, are seen compacts and homogeneous without the presence of voids and with darker and flat oxides between the splats. There are also unmelted particles present, which appear as rounded elements, those characteristics are noted also in the double layer coatings. At the second column are shown three of the five treatments of double layer, can be seen how the button layer increase the thickness and the top coat reduce his thickness.

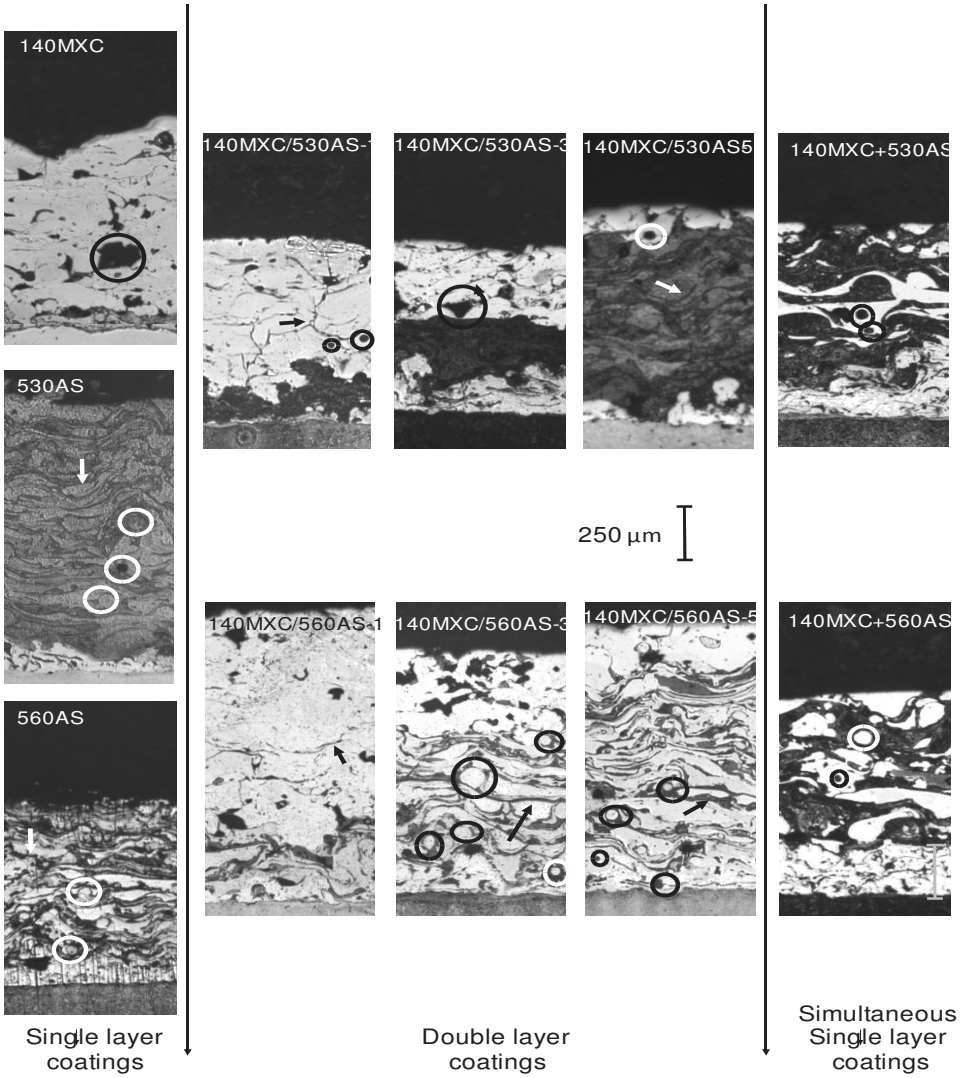

Figure 3. Micrographs (100X) of the deposited coatings for three different morphologies, single layer coatings, double layer coatings ans simultaneous layer coatings.

The Table 2 shows the results of potentiodynamic test [21]. It should be noted that the bilayers exhibit a slight improvement in the corrosion resistance with respect to 140MXC in terms of the current and corrosion potentials. This could be due to the contact of the electrolyte with the interface of the bilayers. However, the polarization for 560AS exhibits the lowest values of corrosion current, which is in good agreement with the stainless nature of this material. The observed curve characteristic of the 530AS sample has a less noble nature in comparison to the cases discussed above. As a manner of reference, it can be observed that the substrate is the least noble of all of the tested materials due to its low nickel and chromium concentrations, which are alloying elements known to significantly improve the corrosion resistance of steels [22-23].It should be emphasized that the characteris of the simultaneous monolayer of 140MXC+530AS increases the corrosion potential with respect to the 530AS coating without significant loss of properties in the 140MXC layer. This effect may be due to the influence of the big difference in chemical compositions it cause that the stabilization of the galvanic corrosion be fast [10, 13]. Finally,the table compare the potentiodynamic polarization of the 140MXC and 560AS monolayers and the simultaneous monolayer, 140MXC+560AS. It can be observed that the mixture of 140MXC+560AS results in a more noble coating than its predecessors; however, there is a significant increase in the corrosion current with respect to 560AS. As in the previous case, this effect may be due to the difference of the chemical composition in the pseudo-alloys however as can be seen at electrochemical impedance spectroscopy the corrosion process is stabilized after some hours showing a different behavior.

In Table 2 also can be observed that the substrate is the least noble material. With respect to the corrosion potential values, both 530AS and 560AS as simultaneous monolayers reduced the activity. The effect on the corrosion current is significant when 560AS is applied in the simultaneous monolayers as can be read in the current column chart for each coating, The current density present in the monolayers of this material is the lowest that of the other coatings and is in agreement with the stainless nature of the AISI 420 steel.

Table 2. Tafel polarization resistance summary.

Coating	Icorr (A)	σI	Ecorr (V)	σV
140MXC	*7.17X10^(-6)*	*2 X10^(-6)*	*-632.5*	*-25*
530AS	*3.10 X10^(-6)*	*1.5 X10^(-6)*	*-799*	*-45*
560AS	*0.45 X10^(-6)*	*8 X10^(-8)*	*-682.25*	*-24*
140MXC+530AS	*4.9 X10^(-6)*	*1.5 X10^(-6)*	*-657.4*	*-7*
140MXC+560AS	*3.50 X10^(-6)*	*2 X10^(-7)*	*-576*	*-6*
AISI 4340	*0.59 X10^(-6)*	*2 X10^(-7)*	*-833.33*	*-5*
140MXC/530AS-(1 to 5)	*≈ 6.85X10^(-6)*	*2 X10^(-6)*	*≈-636.7*	*-27*
140MXC/560AS (1 to 5)	*≈ 7.24X10^(-6)*	*2 X10^(-6)*	*≈-621.5*	*-22*

Figure 4 shows a comparative Bode diagram for all of the coatings involving the 530AS and 140MXC wires. A significant similarity appears between the diagrams for the 140MXC and 140MXC/530AS-3 coatings. The phase angle for these coatings is characterized by two time constants. The first is significantly more pronounced, can be observed on the left-hand side and is generally associated with diffusive phenomena and mass transport. On the right-hand side, a second time constant can be observed and is associated with the corrosion phenomena itself. The polarization resistance increases over time if is extrapolated the curve and that is confirmed in the model made below; this phenomenon can be observed in the upward shifting of the phase angle and the impedance modulus. It also can be observed that the behavior of the 140MXC+530AS simultaneous monolayer exhibits a similar behavior to that of 530AS. Here, the phase angle is shifted to the left, which indicates that the electric polarization due to the concentration of ionic species in the coating surface takes more time,

thereby facilitating the exchange of ions or corrosion [22]. In the impedance modulus, the same shift toward the left can be observed, which confirms the previously described phenomenon.

The second group of coatings was applied, containing the 560AS and 140MXC wires. Figure 5 shows comparatively the Bode diagrams for the 140MXC, 560AS, 140MXC/560AS, and 140MXC+560AS coatings. Similarities can be identified between the Bode diagrams of 140MXC and 140MXC/560AS. Their phase angle diagrams indicate two time constants: one on the left-hand side, associated with diffusive phenomena, and the other on the right-hand side, associated with the corrosion phenomenon. The behavior of the simultaneous monolayer of 140MXC+560AS is similar to that of the 560AS coating. Phase angle shifts and a reduction in the impedance modulus to a frequency of 0.01 Hz are also observed. This result is possibly due to the diffusion of the electrolyte on the coating and to corrosive attack on the surface of the substrate.

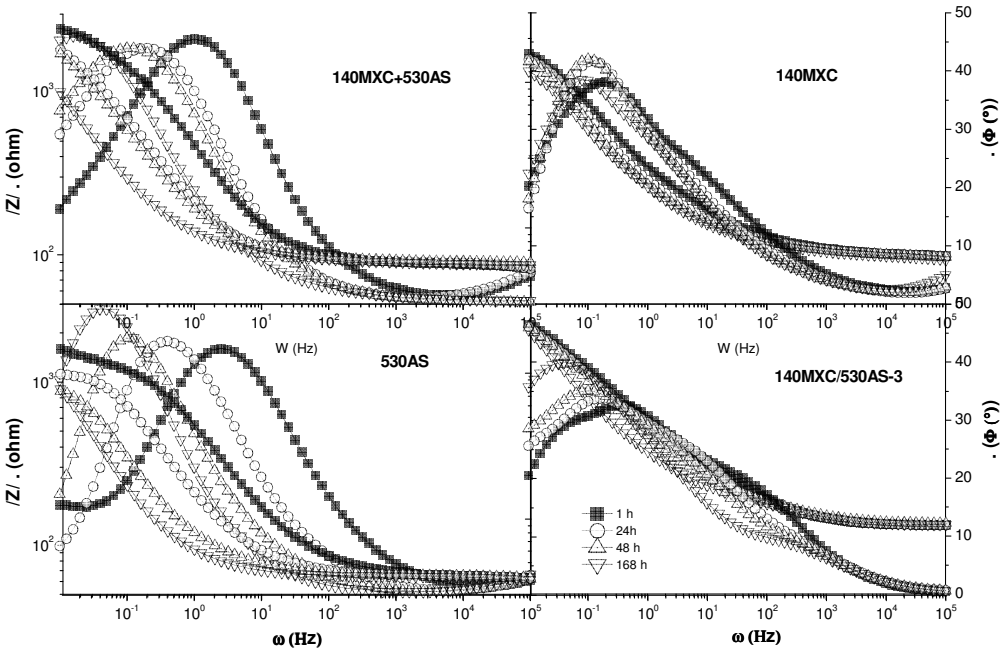

Figure 4. Bode diagrams for the coatings 140MXC+530AS, 140MXC, 530AS, and 140MXC/530AS-3 following 1, 24, 48, and 168 hours.

Figure 6 shows three equivalent circuits for modeling the behavior of the tested coatings: (a) and (b) are essentially basic Randles circuits with and without a Warburg diffusion element. These circuits were properly adjusted to the behavior of the 530AS, 560AS, 140MXC+560AS, and 140MXC+530AS coatings. In this last case, the diffusive effects continue throughout the 168 hours of immersion, while in the other coatings, these effects disappear within the first 24 hours. This disappearance could be due to the stabilization of the corrosion processes [24-26]. The two circuits are typically applied to tests with surfaces possessing a low number of defects, and the effect of corrosion can only be observed with the double layer. The model that best fits the behavior of the 140MXC, 140MXC/530AS-3, and 140MXC/560AS-3 coatings (i.e., the coatings with material from the 140MXC wire at the top of the coating) exhibits two constant phase elements in parallel. As shown in (c), the first capacitance emulates the capacitive effects in pores (Cc), and the second emulates the capacitive effects on the coating surface (Ccor). This model also has three resistive elements, which are associated with the previous capacitances and the electrolyte resistance[22]. This circuit is typically associated with the porous structures and the presence of surface defects and is in agreement with the metallographic measurements.

©2014 Universidad Simón Bolívar

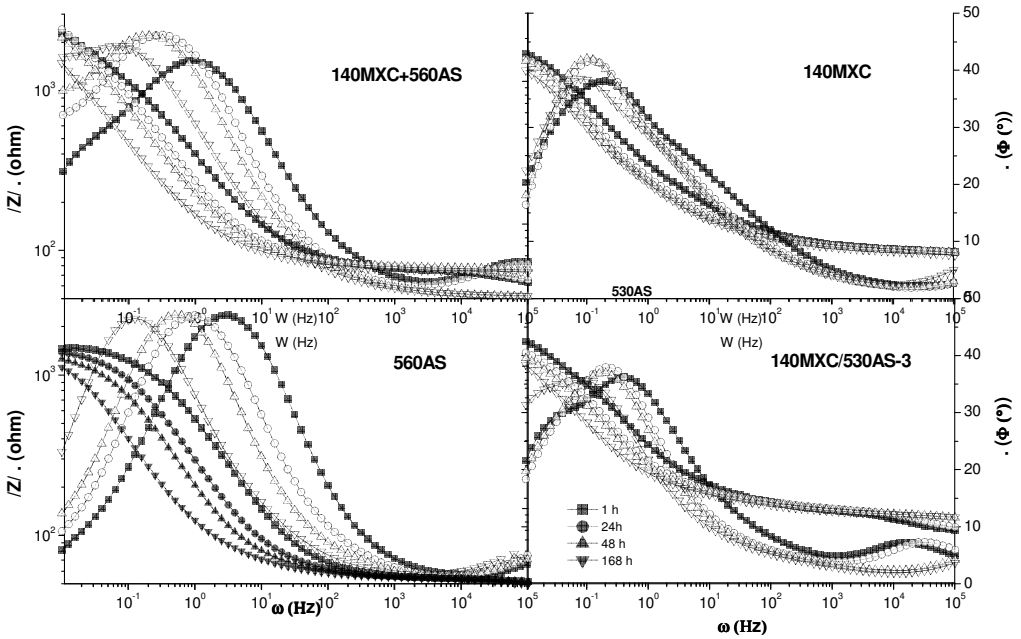

Figure 5. Bode diagrams for the 140MXC+560AS, 140MXC, 560AS, and 140MXC/560AS-3 coatings following 1, 24, 48, and 168 hours.

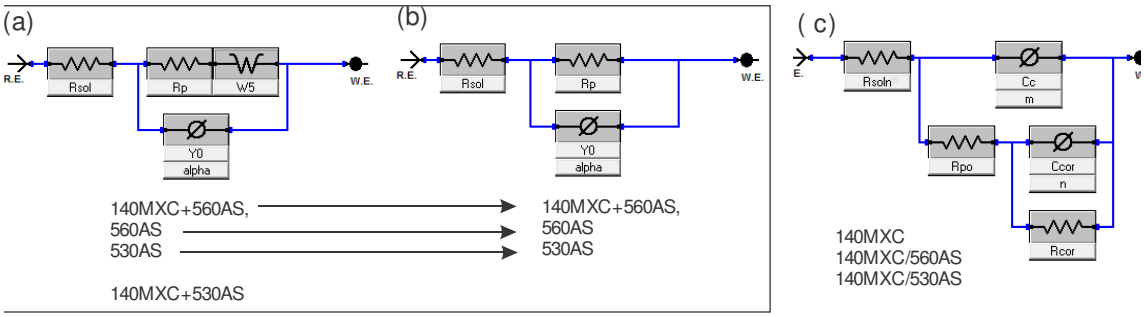

Figure 6. Equivalent circuits of (a) the circuit modeling simultaneous single layer coatings 140MXC+530AS and for the first day 140MXC+560AS, single layers 560AS, 530AS (b) the model of 140MXC+560AS,560AS and 530AS (c) the model for single layer 140MXC and double layer coatings 140MXC/560AS.

Finally the Figure 7 shows some results of the equivalent circuits applied to the polarization resistance "Rp", can be seen that the double layer coatings increased significantly the polarization resistance with respect to their precursors, the effect being greater in 140MXC 530 regarding to the 530AS single coating. Metallographic observations, tests, equivalent circuits and modeled results possibly indicate that there were two corrosion mechanisms defined by the two groups of equivalent circuits.

The first model is applied to conventional steel single coatings, as well as simultaneous single layer coatings where corrosion could be located within the boundary of splats, because this is a high energy boundary [4, 23, 27], also the oxides between splats promote preferably the corrosion , the corrosion is not at inside the coating due to there are no open surface defects like cracks or porosities, the equivalent circuit is changed after the first few hours due to stabilizing corrosive processes , this is evidenced by the disappearance of diffusive processes modeled by Warburg elements.

With respect to the single coating 140MXC and double layer coating, is proposed that the observed cracks connected together at the outside of coating let to the electrolyte penetrate as the time passes. This phenomenon can be observed at the polarization assays on the single 140MXC and double coatings with similar results, while the results of electrochemical impedance test change with respect to time for both types of coatings, that could indicate that it takes time to penetrate across the cracks and get lower, increased Rp could indicate that the electrolyte reached underlayment and corrosion products clog the defects, the same effect was observed by authors like Jianguo [24].

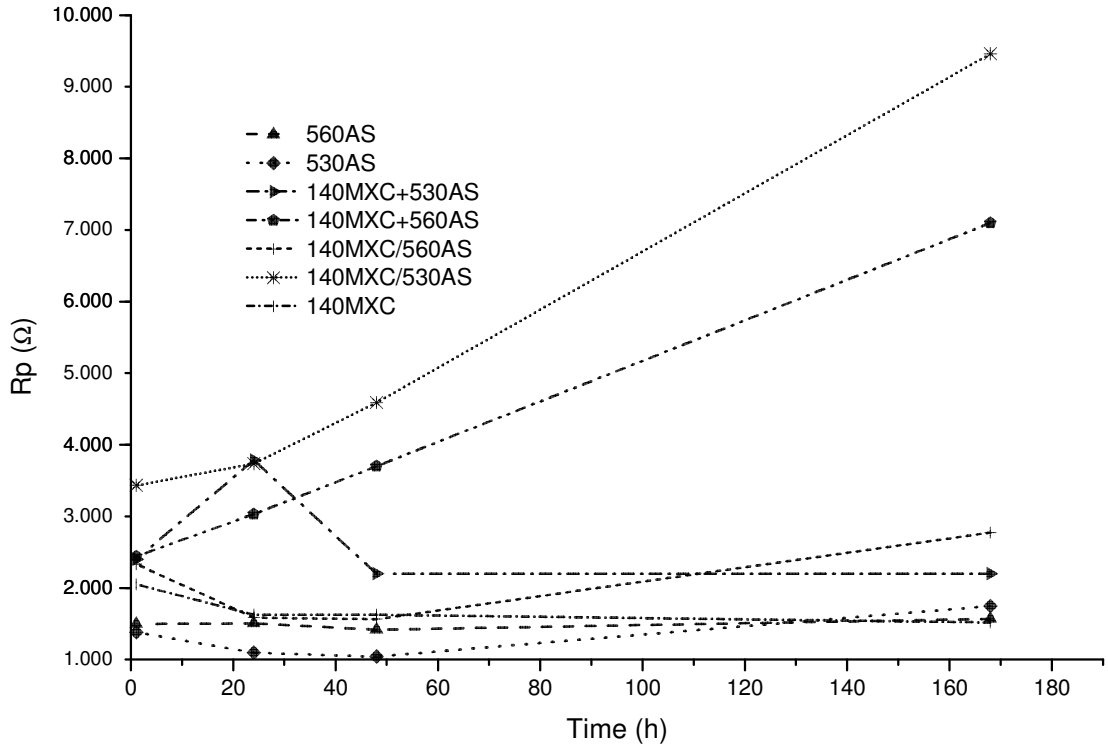

Figure 7. Polarization resistance of coatings modeled using data from Figures 4-5 and the model in the Figure 6.

4. CONCLUSIONS

Pseudo-alloys or mechanical mixtures of materials were obtained in simultaneous monolayers. These monolayers were characterized by chemical component mixtures and significant reductions in defects with respect to 140MXC.The polarization resistance was increased in the bilayers due to the congestion of defects with corrosion products, thus indicating the need to improve the coating conditions for 140MXC. Finally the corrosion resistance of the 140MXC+530AS and 140MXC+560AS coatings improved the corrosion potential of 530AS and 560AS without significantly modifying this property with respect to 140MXC. An incremental increase in the corrosion current of coating 560AS was observed. Finally, the bilayer-type coatings increased the polarization resistance by clogging the 140MXC defects.

5. ACKNOWLEDGEMENTS

The authors are grateful to Colciencias for the financial support for this research through the project “Resistencia a la corrosión y al desgaste de recubrimientos para aplicaciones en la industria naval aplicados por la técnica de proyección termica” and Jairo Olaya thanks Alfredo Morales and Pedro Rondón of the company Cotecmar for their collaboration in this research.

©2014 Universidad Simón Bolívar

6. REFERENCES

[1] Deshpande S, Sampath S, Zhang H, Surf. Coat. Tech. 2006; 200 (12): 5395-5406

[2] Newbery A, Grant P, J. Mater. Process. Tech. 2006; 178 (11): 259-269.

[3] Rabiei A, Mumm D, Hutchinson J, Schweinfest R, Rühle M, Evans A, Mater. Sci. Eng. 1999; 269 (14): 152-165.

[4] Thermal Spray Society Training Committee. Handbook of Thermal Spray Technology. J.R. Davis Davis & Associates 1st ed. ohio (EE.UU): ASM International®, 2004.

[5] Jin G, Xu B, Wang H, Li Q, Wei S, Surf. Coat. Tech. (2007); 201 (3): 5261-5263.

[6] Edrisy A, Perry T, Cheng Y, Alpas A, Surf. Coat. Tech. 2001; 146-147 (7): 338-334.

[7] Edrisy A, Alpas A, Thin. Solid. Films. 2002; 420-421 (7): 338-334.

[8] Edrisy A, Perry T, Cheng Y, Alpas A, Wear. 2001; 251 (11): 1023-1033.

[9] Dimaté L, Ortíz M, Morales J, Olaya J, IBEROMET XI X CONAMET/SAM, Viña del mar (Chile) IBEROMET 2010.

[10] Barbara A, Shaw M, Leimkuhler P, Moran, J. "Corrosion Performance of Aluminum and Zinc-Aluminum Thermal Spray Coatings in Marine Environments" Testing of Metallic and Inorganic Coatings, ASTM STP 947 Harding W, Bari G, ASTM 1987 246-264.

[11] Robert M, Kain, Earl A, "Marine Atmospheric Corrosion Museum Report on the Performance of Thermal Spray Coatings on Steel" Testing of Metallic and Inorganic Coatings, ASTM STP 947 Harding W, Bari G, ASTM 1987 211-234.

[12] Lin B, Lu X, Li L, T. Nonferr. Metal. Soc. 2009; 19 (6) :1556-1561.

[13] Pokhmurs'kyi V, Dovhunyk V, Sydorak I, Mater. Sci+. 2002; 38 (3): 455-457.

[14] ASM International Handbook Committee, Vol 1 Properties and Selection 10 ed. ohio ASM International®, 1993 (EE.UU).

[15] Mellali M, Grimaud A, Leger A, Fauchai P, Lu J, Asm. Int. 1997; 6(11) : 217-227.

[16] Wang Y, Li C, Ohmori A, Thin. Solid. Films. 2005; 485 (7): 141-147.

[17] Patel K, Doyle C, Yonekura D, James B, Surf. Coat. Tech. 2010; 204 (6): 3567-3572.

[18] Norma ASTM G5-04, Standard Reference test for making potentiostatic and potentiodynamic anodic polarization measurements, Pennsylvania (EE.UU): American Society for Testing and Materials, 2004.

[19] Norma ASTM G3-10, Standard Practice for Conventions Applicable to Electrochemical Measurements in Corrosion Testing, Pennsylvania (EE.UU): American Society for Testing and Materials, 2010.

[20] Norma ASTM 407-11, Standard Practice for Microetching Metals and Alloys, Pennsylvania (EE.UU): American Society for Testing and Materials, 2011.

[21] Lopez E, Flórez O, Ingeniería E Investigación. 2013; 33 (6): 23-28.

[22] Kelly G, Scully R, Shoesmith W, Buchheit G. Electrochemical Techniques in Corrosion Science and Engineering. 1ed. New York,: Marcel Dekker, Inc, 2002. (EE.UU).

[23] ASM International. Corrosion Understanding The Basics. 1 ed. Ohio: J.R. Davis Davis & Associates, 2000, (EE.UU).

[24] Jianguo L, Gaoping G, Chuanwei Y, Electrochim. Acta. 2005; 50 (13): 3320-3332.

[25] Liu C, Bi Q, Leyland A, Matthews A, Corros. Sci. 2003; 45 (14): 1243-1256.

[26] Stansbury E, Buchanan E. Fundamentals of Electrochemical Corrosion. 1ed. ASM International®, 2000, (EE.UU).

[27] Pierre R, Handbook of Corrosion Engineering. 1 ed. New York: McGraw-Hill, 1999. (EE.UU)

©2014 Universidad Simón Bolívar